Current Research in Physiology 6 (2023) 100106

Contents lists available at ScienceDirect

Current Research in Physiology

journal homepage: www.sciencedirect.com/journal/current-research-in-physiology

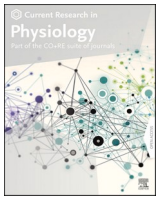

Dopamine transporter membrane mobility is bidirectionally regulated by phosphorylation and palmitoylation

Madhur Shetty, Danielle E. Bolland [1], Joshua Morrell, Bryon D. Grove, James D. Foster [*], Roxanne A. Vaughan [*]

Department of Biomedical Sciences, University of North Dakota, School of Medicine and Health Sciences, Grand Forks, ND, 58202, USA

ARTICLE INFO

Keywords:
Fluorescence recovery after photobleaching
FRAP
Protein kinase C
Mitogen activated protein kinase
Palmitoyl acyl transferase
DHHC2
Amphetamine
2-Bromopalmitate

ABSTRACT

The primary regulator of dopamine availability in the brain is the dopamine transporter (DAT), a plasma membrane protein that drives reuptake of released dopamine from the extracellular space into the presynaptic neuron. DAT activity is regulated by post-translational modifications that establish clearance capacity through impacts on transport kinetics, and dysregulation of these events may underlie dopaminergic imbalances in mood and psychiatric disorders. Here, using fluorescence recovery after photobleaching, we show that phosphorylation and palmitoylation induce opposing effects on DAT lateral membrane mobility, which may influence functional outcomes by regulating subcellular localization and binding partner interactions. Membrane mobility was also impacted by amphetamine and in polymorphic variant A559V in directions consistent with enhanced phosphorylation. These findings grow the list of DAT properties controlled by these post-translational modifications and highlight their role in establishment of dopaminergic tone in physiological and pathophysiological states.

1. Introduction

In the brain, dopamine (DA)[3] controls numerous functions including cognition, mood, and reward, and dysregulation of signaling is linked to the etiology of numerous motor and psychiatric disorders. The availability of DA for neurotransmission is controlled by the dopamine transporter (DAT), a 12-transmembrane domain protein expressed on the plasma membrane of dopaminergic neurons (Nirenberg et al., 1996). DAT actively transports released transmitter from the extracellular space into presynaptic neurons and is the major determinant for physiological control of DA signaling and homeostasis (Giros et al., 1996). DAT mediates the addictive properties of many psychostimulant drugs including cocaine, amphetamine (AMPH), and methamphetamine (METH), and is a target for pharmacotherapies such as Adderall and Ritalin prescribed for attention deficit hyperactivity disorder (ADHD), autism spectrum disorder (ASD), bipolar disorder (BD), and other dopaminergic pathologies. Some drugs such as cocaine directly inhibit uptake, whereas others including AMPH and METH are substrates that stimulate efflux of intracellular DA via reverse transport. Both processes lead to transmitter overflow and govern the strength of DA signaling during drug abuse and therapeutic treatment.

The transport capacity of DAT is under tight control by presynaptic signaling pathways, and dysregulated reuptake is suspected to contribute to spatial and temporal transmitter imbalances in drug addiction and disease states (Bermingham and Blakely, 2016; Schmitt and Reith, 2010; Vaughan and Foster, 2013). The mechanisms underlying these regulatory events are complex and overlapping, and include control of transport kinetics and regulation of transporter plasma membrane levels. The specific details of these processes are largely unknown, but include post-translational mechanisms that modulate phosphorylation and palmitoylation of the transporter or its regulatory partners.

Phosphorylation of DAT is most well-characterized with respect to protein kinase C (PKC), which catalyzes modification of multiple serine residues at the distal end of the cytoplasmic N-terminus, and mitogen activated protein kinases (MAPKs) that are coupled to human (h) and rat (r) proline-directed residues Ser53/Thr53 in the membrane proximal region of the N-terminus (Foster and Vaughan, 2017; Vaughan and Foster, 2013). Phosphorylation of PKC-domain residues induces kinetic down-regulation of transport and enhancement of efflux (Bowton et al., 2010; Khoshbouei et al., 2004; Moritz et al., 2015), whereas Thr53 phosphorylation induces transport upregulation mediated by MAPK-coupled kappa opioid and D2 DA receptors (Bolan et al., 2007;

* Corresponding authors.
E-mail addresses: james.d.foster@und.edu (J.D. Foster), roxanne.vaughan@und.edu (R.A. Vaughan).
[1] Current address: Division of Science and Math, University of Minnesota, Morris, Morris, MN 56267.

https://doi.org/10.1016/j.crphys.2023.100106
Received 12 May 2023; Accepted 20 September 2023
Available online 29 September 2023

The abbreviations used are

DA	dopamine
DAT	dopamine transporter
FRAP	fluorescence recovery after photobleaching
PKC	protein kinase C
MAPK	mitogen activated protein kinase
AMPH	amphetamine
METH	methamphetamine
PMA	phorbol 12-myristate, 13-acetate
2BP	2-bromopalmitate
ADHD	attention deficit hyperactivity disorder
ASD	autism spectrum disorder
BP	bipolar disorder

Gowrishankar et al., 2018; Mayer et al., 2023). Thr53 phosphorylation is also implicated in substrate efflux (Foster et al., 2012; Wang et al., 2016) and is indirectly stimulated by PKC through MAPK pathway cross-talk (Wetzker and Böhmer, 2003). Dysregulation of transporter phosphorylation is linked to drug mechanisms, as AMPH and METH increase phosphorylation of PKC and Thr53 domain residues through upstream activation of PKC (Challasivakanaka et al., 2017; Foster et al., 2012). Phosphorylation also occurs on other less well-characterized N-terminal residues (Yang et al., 2019), and how information from all sites is integrated is not known, indicating a complex and incompletely understood role for N-terminal modification in modulating transport capacity.

DAT also undergoes rapid and reversible S-palmitoylation, the addition of a lipid moiety to SH groups of intracellularly accessible cysteine residues, catalyzed by palmitoyl acyl transferase (DHHC) enzymes. This modification induces kinetic upregulation of surface transporters and increases total transporter levels through inhibition of degradation (Foster and Vaughan, 2011; Rastedt et al., 2017). Palmitate addition occurs at multiple sites, with a significant fraction present on r/hDAT residues Cys580/581 at the membrane-cytoplasm interface of transmembrane domain 12. PKC suppresses the tonic level of palmitoylation, and Cys580 palmitoylation and Ser7 phosphorylation are mechanistically linked, with each modification inhibiting the other to coordinately regulate transport velocity (Moritz et al., 2015). Details of how palmitoylation and phosphorylation synergize to reciprocally regulate transport kinetics remain to be elucidated, but likely involve impacts on intracellular aspects of the permeation pathway.

Cholesterol and other lipids also play key roles in DAT function (Khelashvili and Weinstein, 2015; Piniella et al., 2021), and transporter phosphorylation occurs preferentially in cholesterol-rich membrane rafts, suggesting a link between membrane and post-translational mechanisms (Foster and Vaughan, 2011). Here we now use fluorescence recovery after photobleaching (FRAP) to examine the role of phosphorylation and palmitoylation in transporter lateral membrane mobility, using pharmacological, enzyme co-expression, and mutagenesis approaches to promote various DAT forms. We also examined the properties of hDAT A559V, a coding variant identified in individuals diagnosed with ADHD, ASD, and BD, which displays endogenously enhanced phosphorylation and tonically elevated efflux that may contribute to the disease phenotype (Bowton et al., 2010, 2014).

Our findings show that DAT lateral membrane mobility is enhanced by conditions promoting phosphorylation and reduced by conditions promoting palmitoylation, with enhanced mobility consistent with elevated phosphorylation found with AMPH treatment and in the A559V variant. These results indicate that transporter membrane properties represent crucial elements in physiological and pathophysiological control of reuptake.

2. Materials and methods

2.1. DNA constructs

Plasmids containing coding sequence for enhanced yellow fluorescent protein (EYFP)-tagged WT DATs were generated by insertion of the WT hDAT or rDAT coding sequence between the *Kpn*I and ECoR I endonuclease cleavage sites in an EYFP-C1 (Clontech) vector. Plasmids containing the coding sequence for EYFP-tagged DAT mutants were generated by codon substitution in the EYFP-C1 vector containing WT hDAT or rDAT sequences using the Stratagene QuikChange® Kit with appropriate primers. HA-tagged human DHHC2 and DHHC11 coding plasmids in pEF-BOS-HA vector were the generous gift of Dr. Masaki Fukata (Fukata et al., 2004). The DHHA2 construct was generated from the DHHC2 cDNA template by mutating Cys 156 to alanine using the Stratagene QuikChange® Kit with appropriate primers (Bolland et al., 2019). All codon substitutions were verified by sequencing (Eurofins MWG).

2.2. Cell culture and transient transfection

Neuro 2a (N2a) mouse neuroblastoma or Lilly lab cell-porcine kidney ($LLCPK_1$) cells were transiently transfected with the indicated EYFP-DAT vectors to express the corresponding DAT proteins. Cells were grown in 12-well culture plates and transfected with 1.4 μg plasmid/well using XtremeGene transfection reagent (Roche) in a 3:2 ratio. FRAP experiments were performed using cells seeded on 1 mm glass coverslips 24–48 h post transfection. Cells were maintained in Dulbecco's modified eagle's medium (DMEM) supplemented with 10% FBS and 1X penicillin/streptomycin and incubated in a humidified chamber gassed with 5% CO_2 at 37 °C. DAT expression level in transfected cells was verified by sodium dodecyl sulfate-polyacrylamide gel electrophoresis followed by immunoblotting of cellular lysates against DAT specific antibodies as previously described (Foster et al., 2012; Moritz et al., 2015) (not shown) and by fluorescence confocal microscopy. Co-transfection of rDAT with DHHC constructs was performed as described (Bolland et al., 2019).

2.3. Confocal microscopy and fluorescence recovery after photobleaching (FRAP)

FRAP analysis of EYFP-tagged WT or mutant r/hDATs was performed using a Zeiss 510 META laser scanning confocal microscope. For each FRAP run, cells were excited at 514 nm with an argon laser (2% power) through a 100X 1.45 NA oil immersion objective and imaged using a 530 nm long pass emission filter. A series of images was captured at ~4 s intervals to establish a fluorescence intensity baseline for a 1.32 μm diameter circular region of interest (ROI) corresponding to the size of the bleach area on the cellular plasma membrane. The ROIs were then photobleached at 514 nm with an argon laser (100% power). Following photobleaching, a total of 100 images was captured for analysis of FRAP using ImageJ software. After correction for photobleaching during image capture, fluorescence recovery vs time for each cell was plotted using GraphPad Prism software and subjected to nonlinear regression analysis using an exponential recovery function ($F(x) = A\ (1\text{-}\exp\ (-\tau x)) + c$) where $A + c$ is the normalized maximum intensity value at recovery, τ is a fitted parameter, x is the time after bleaching, and c is the offset value. $T_{1/2}$ was determined by the equation $T_{1/2} = \ln 0.5/-\tau$ and diffusion coefficients (D, $\mu m^2/s$) were calculated using $0.244\ r^2/T_{1/2}$ where r is the radius of the ROI and $T_{1/2}$ is determined from the nonlinear regression analysis of each recovery curve (Kang et al., 2012). Experiments were performed three or more times with three or more independent cells per experiment. Results are reported as mean ± standard error (S.E.), and statistical analyses were performed using unpaired Student's t-test or ANOVA with Fisher LSD or Tukey post-test as indicated.

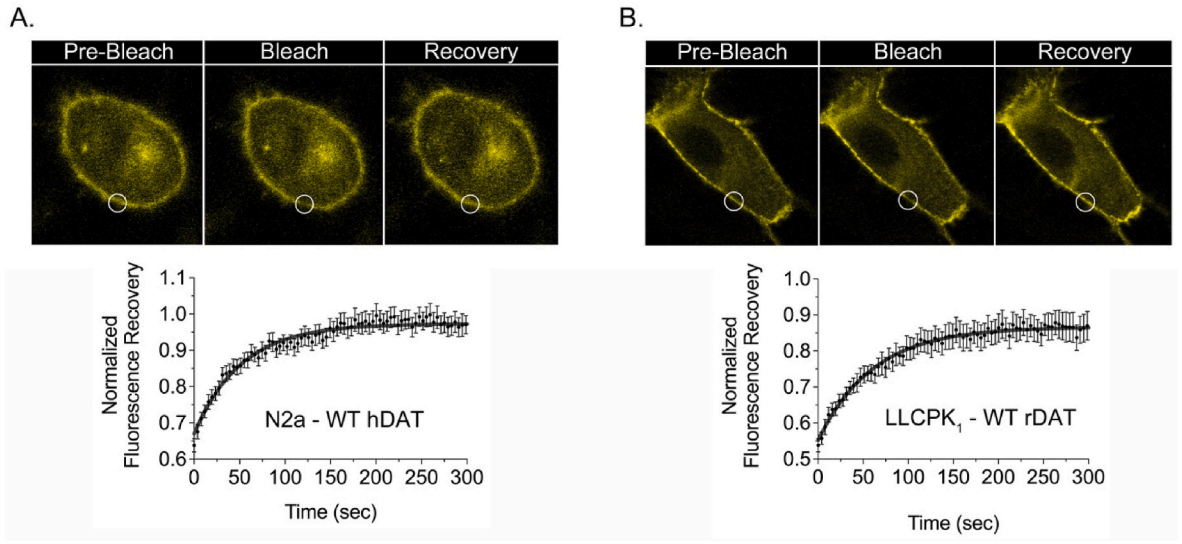

Fig. 1. FRAP characteristics of DAT in N2a and $LLCPK_1$ cells. (A) N2a cells transiently transfected with EYFP-hDAT or (B) $LLCPK_1$ cells transiently transfected with EYFP-rDAT were subjected to FRAP analysis. Sequences show representative confocal images of DAT in pre-bleach, bleach, and recovery conditions with circles indicating the region of bleaching. Graphs show a representative recovery curve (means ± S.E.) from independent experiments for each cell type.

2.4. Pharmacological treatments

For phosphorylation studies, cells were treated at 37 °C with vehicle or 1 μM PMA for 30 min, or with vehicle or 10 μM AMPH for 20 min prior to confocal imaging and FRAP analysis. For palmitoylation studies, cells were treated at 37 °C with vehicle or 15 μM 2-bromopalmitate (2BP) for 3 h prior to confocal imaging and FRAP analysis.

2.5. Materials

DMEM, G418 sulfate, 1X penicillin/streptomycin, and L-glutamine were from Corning Cellgro (Manassas, VA, USA); FBS was from Atlanta Biologicals (Atlanta, GA, USA); XtremeGene transfection reagent was from Roche (Indianapolis, IN, USA); AMPH and 2BP were from Sigma Aldrich (St. Louis, MO, USA), PMA was from Calbiochem (San Diego, CA, USA).

3. Results

Membrane mobility of human (h) and rat (r) DATs was examined using FRAP analysis of EYFP-tagged WT and mutant forms expressed in N2a or $LLCPK_1$ cells. Fig. 1A and B shows representative FRAP analyses of EYFP-hDAT expressed in N2a cells and EYFP-rDAT expressed in $LLCPK_1$ cells. In both cell lines DAT is predominantly expressed at the plasma membrane with lower levels in internal vesicles, and the same general distribution was seen with mutant forms, pharmacological

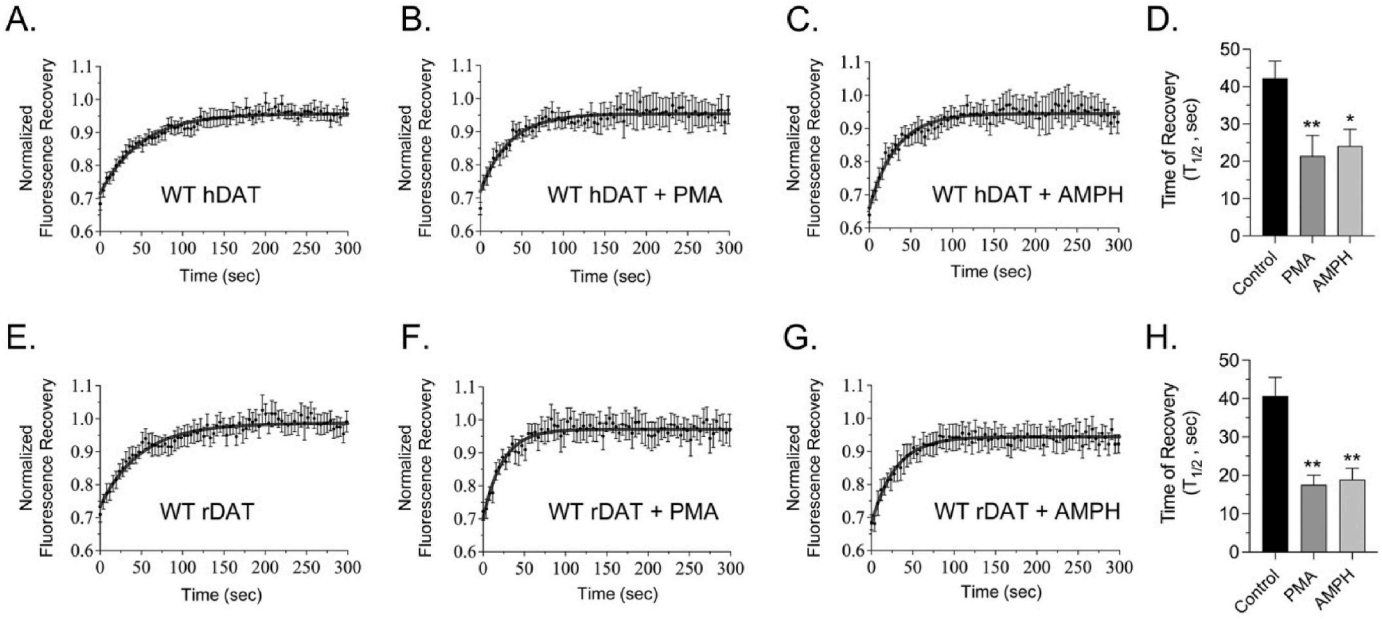

Fig. 2. Phosphorylation conditions increase DAT lateral membrane mobility. N2a cells expressing WT hDAT (A–C) or WT rDAT (E–G) were treated with vehicle, PMA (1 μM, 30 min), or AMPH (10 μM, 20 min) and subjected to FRAP analysis. Graphs show summary recovery curves (means ± S.E.) for independent experiments for each form. (D and H), Quantification of FRAP recovery times ($T_{1/2}$, sec) for each condition (means ± S.E. of 3 or more independent experiments using 3 or more cells/experiment); *$p < 0.05$, **$p < 0.01$ indicated conditions vs. control (one-way ANOVA with Fisher's LSD post test).

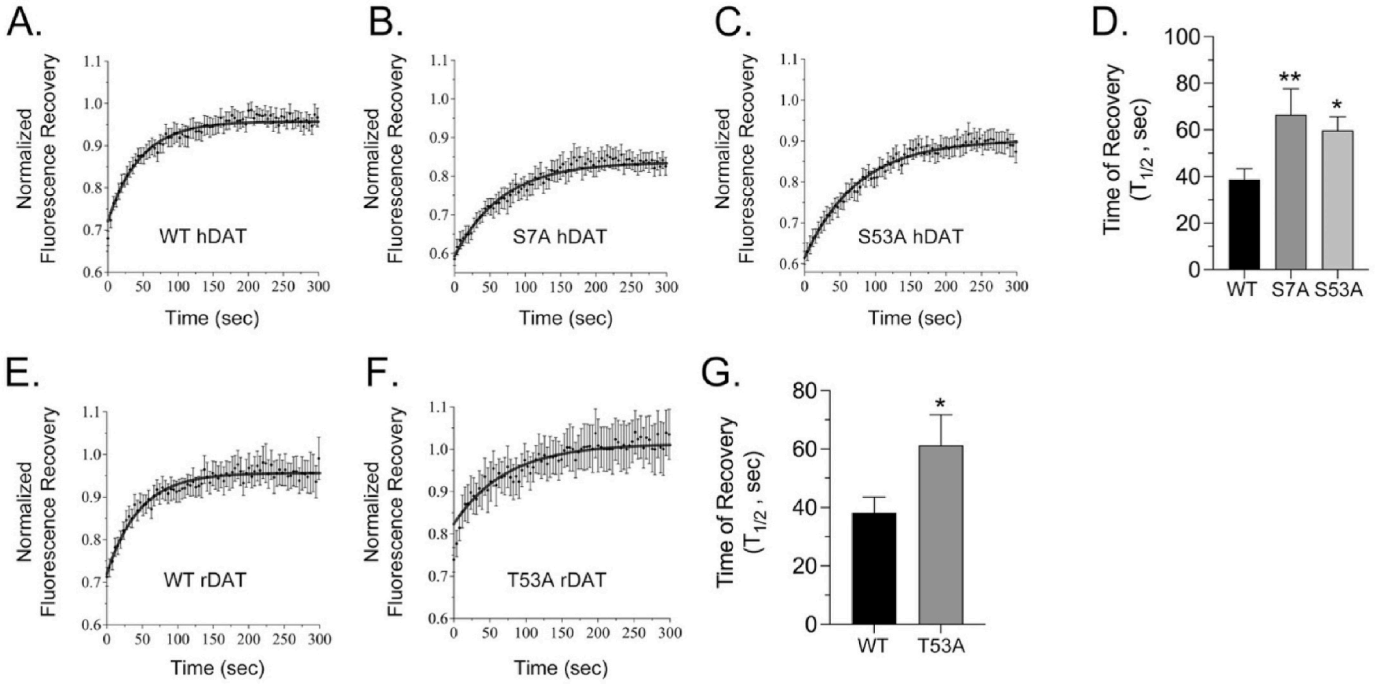

Fig. 3. Phosphorylation site mutations reduce DAT lateral membrane mobility. N2a cells expressing the indicated EYFP-hDAT forms (A–C) or EYFP-rDAT forms (E–F) were subjected to FRAP analysis. Graphs show summary recovery curves (means ± S.E.) for independent experiments for each form. (D and G), Quantification of FRAP recovery times ($T_{1/2}$, sec) for each condition, (means ± S.E. of 3 or more independent experiments, using 3 or more cells/experiment); *p < 0.05, **p < 0.01, indicated DAT forms vs. WT (hDAT, one-way ANOVA with Fisher's LSD post test; rDAT, Student's t-test).

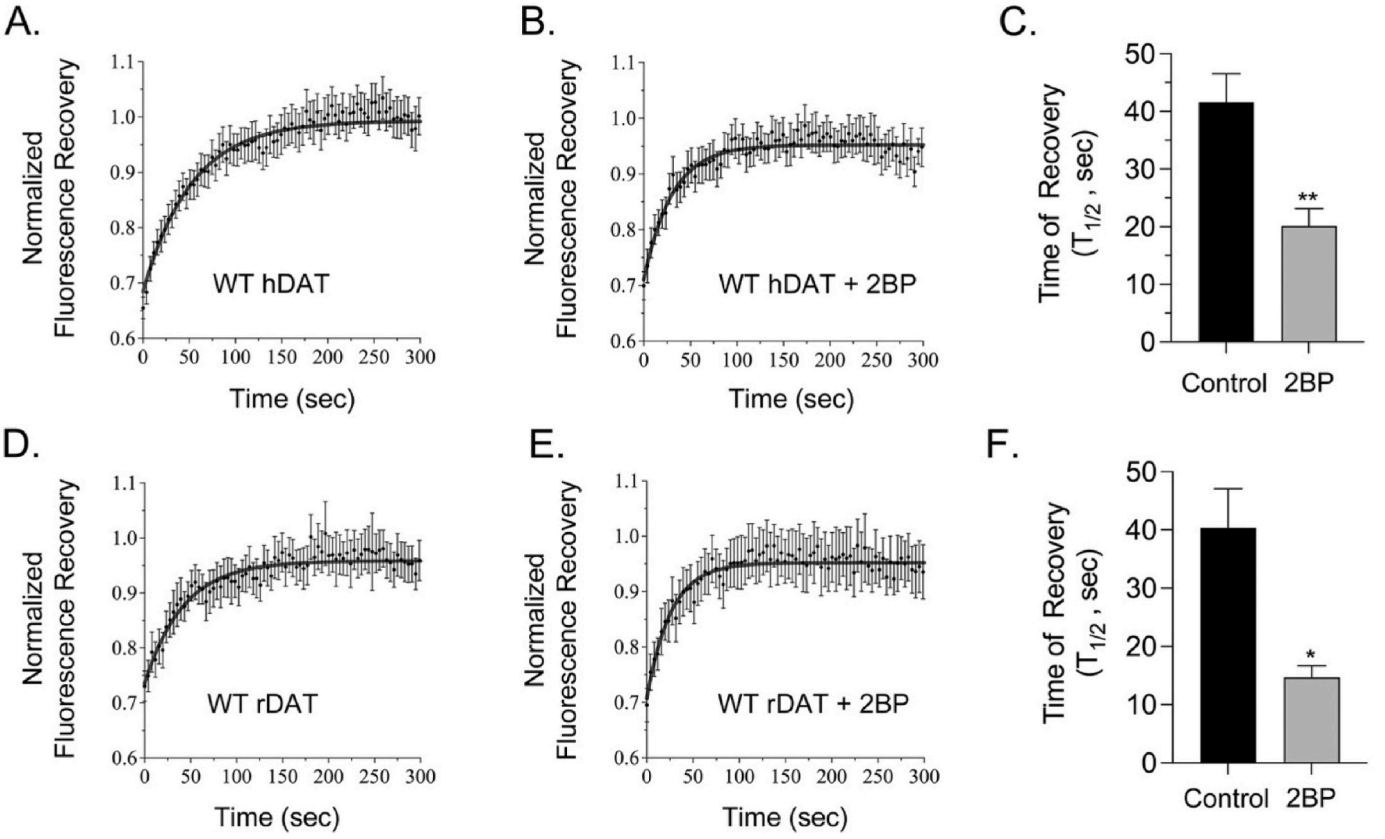

Fig. 4. Pharmacological inhibition of palmitoylation increases DAT lateral membrane mobility. N2a cells expressing EYFP-hDAT (A–B) or EYFP-rDAT (D–E) were treated with vehicle (A, D) or 2BP (15 μM, 3h) (B, E) and subjected to FRAP analysis. Graphs show summary recovery curves (means ± S.E.) for independent experiments for each condition. (C and F), Quantification of FRAP recovery times ($T_{1/2}$, sec) for each condition, (means ± S.E. for 3 or more independent experiments, using 3 or more cells per experiment); *p < 0.05, **p < 0.01, 2BP vs. control (Student's t-test).

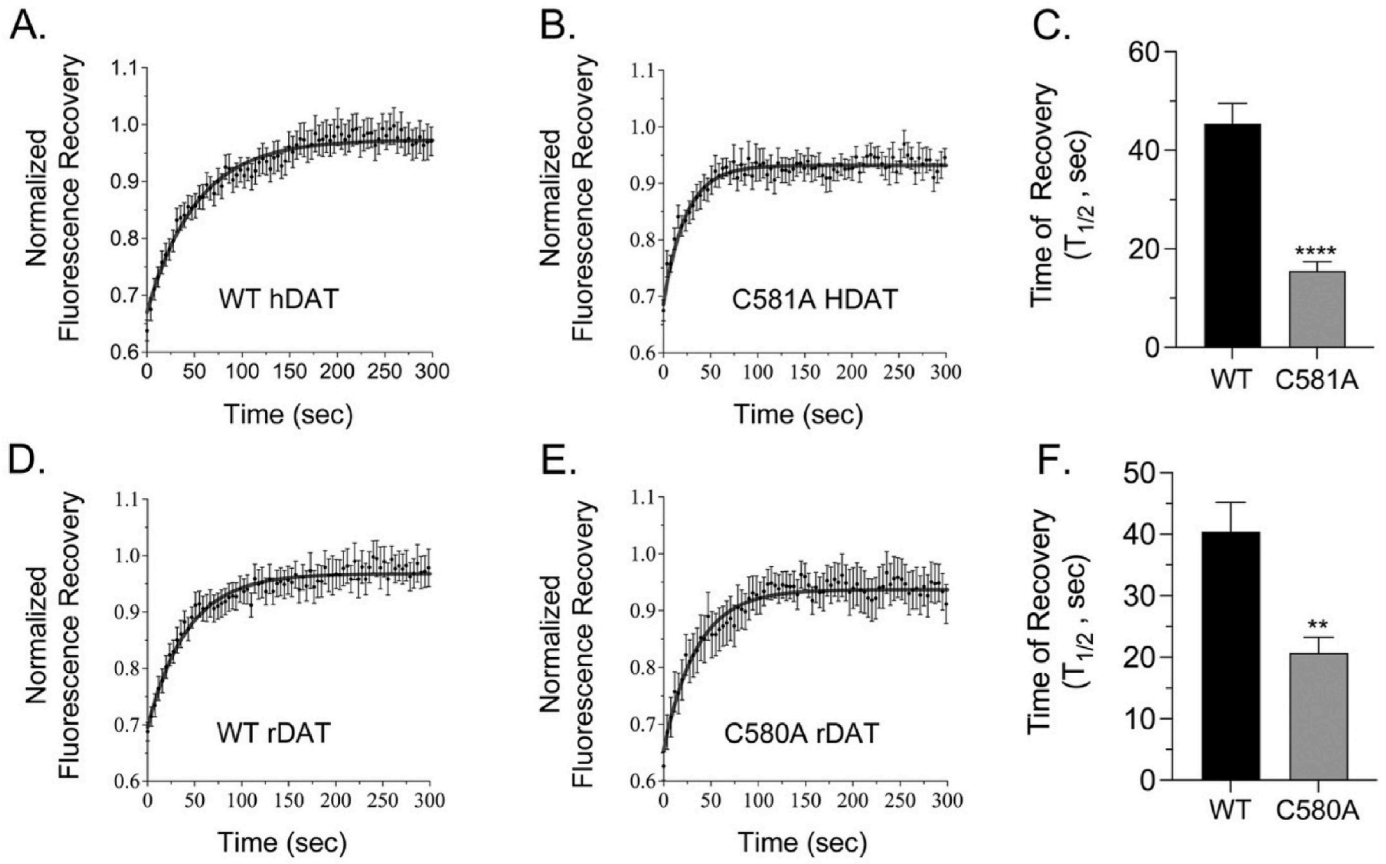

Fig. 5. Genetic inhibition of palmitoylation increases DAT lateral membrane mobility. N2a cells expressing the indicated EYFP-hDAT forms (A–B) or EYFP-rDAT forms (D–E) were subjected to FRAP analysis. Graphs show summary recovery curves (means ± S.E.) for independent experiments for each form. (C and F), Quantification of FRAP recovery times ($T_{1/2}$, sec) for each form (means ± S.E. for 3 or more independent experiments, using 3 or more cells/experiment); **p < 0.01, ****p < 0.0001, indicated DAT forms vs. WT (Student's t-test).

treatments, or enzyme co-expression. The sequences show pre-bleach, bleached, and recovery stages, with the circle indicating the bleached region. Bleaching conditions were selected to reduce fluorescence to ~70% of the starting value. Representative FRAP recovery curves for these DAT forms are shown under the images. Recovery of fluorescence began within seconds and plateaued at ~90% of the starting value between ~100 and 150 s, indicating that DAT possesses significant lateral membrane mobility.

The $T_{½}$ for recovery of WT transporters was highly consistent across individual experiments, with hDAT values ranging from 38.7 ± 4.6 to 45.4 ± 4.2 s (mean = 40.4 ± 3.4 s) and rDAT values ranging from 30.7 ± 3.6 to 41.3 ± 4.1 s (mean = 40.7 ± 4.1 s). The calculated diffusion coefficients (D) for hDAT ranged from 2.9 ± 0.3 to 3.8 ± 0.6 × 10^{-3} $\mu m^2/s$ (mean = 3.3 ± 0.3 × 10^{-3} $\mu m^2/s$) and for rDAT ranged from 3.6 ± 0.4 to 4.7 ± 0.5 × 10^{-3} $\mu m^2/s$ (mean = 4.2 ± 0.4 × 10^{-3} $\mu m^2/s$). These mobility values are similar to those reported utilizing FRAP for YFP-hDAT expressed in N2a and HEK293 cells (Adkins et al., 2007), and for DATs imaged with cocaine analog-conjugated fluorescent or quantum dot tags in neurons, HEK 293 cells, and SK-N-MC cells (Eriksen et al., 2009; Kovtun et al., 2019).

For the experimental conditions examined in Figs. 2–7 we show responses of hDAT and/or rDAT forms expressed in N2a cells. Each figure shows a nonlinear regression curve for the indicated conditions fit to summary recovery data for all cells examined, with each point representing the mean ± S.E. of three independent experiments performed using three or more cells per experiment. Histograms show means ± S.E. of $T_{1/2}$ values determined from individual cell recovery data. Tables 1 and 2 summarize the $T_{½}$ values, diffusion coefficients, and statistical levels for each h/rDAT group from these experiments. Some studies were also performed in $LLCPK_1$ cells, with the values from those experiments presented in Table 3.

Fig. 2 shows the response of DAT membrane mobility to conditions that enhance transporter phosphorylation. N2a cells expressing EYFP-hDAT or EYFP-rDAT were treated with the PKC activator phorbol 12-myristate, 13-acetate (PMA), or with AMPH, using conditions that are well-characterized to stimulate phosphorylation of DAT N-terminal residues (Cervinski and Vaughan, 2005; Challasivakanaka et al., 2017; Foster et al., 2002; Huff et al., 1997). In hDAT cells treated with vehicle (Fig. 2A), the $T_{½}$ for FRAP recovery was 42.2 ± 4.6 s, but with PMA treatment (Fig. 2B) the $T_{½}$ was reduced to 21.4 ± 5.5 s ($p < 0.01$ vs control) and with AMPH treatment (Fig. 2C) the $T_{½}$ was 24.1 ± 4.5 s ($p < 0.05$ vs. control) (Fig. 2D), indicating enhanced mobility in phosphorylation conditions. For rDAT the results were similar, with $T_{½}$ values of 40.7 ± 4.9 s for vehicle (Figs. 2E), 17.6 ± 2.5 s for PMA (Fig. 2F) ($p < 0.01$ vs control), and 18.9 ± 2.9 s for AMPH (Fig. 2G) ($p < 0.01$ vs control) (Fig. 2H).

In Fig. 3 we examined FRAP properties of h/rDAT phosphorylation-null (S/T→A) mutants of Ser7, Ser53, and Thr53, sites which undergo enhanced phosphorylation in response to PMA, AMPH, METH, or are implicated in regulatory responses (Cervinski et al., 2005; Challasivakanaka et al., 2017; Moritz et al., 2013, 2015; Thal et al., 2019). For WT hDAT (Fig. 3A), the $T_{½}$ was 38.7 ± 4.6 s, for S7A (Fig. 3B) the $T_{½}$ was 66.6 ± 11.1 s ($p < 0.01$ vs WT control), and for S53A (Fig. 3C) the $T_{½}$ was 53.9 ± 6.0 s ($p < 0.05$ vs WT control) (Fig. 3D), indicating that membrane mobility is reduced in transporters lacking phosphorylation at these sites. Similarly, the $T_{½}$ for WT rDAT (Fig. 3E) was 38.2 ± 5.4 s, and for T53A (Fig. 3F) was 61.2 ± 10.5 s ($p < 0.05$) (Fig. 3G). Together these findings suggest that phosphorylation of N-terminal domain

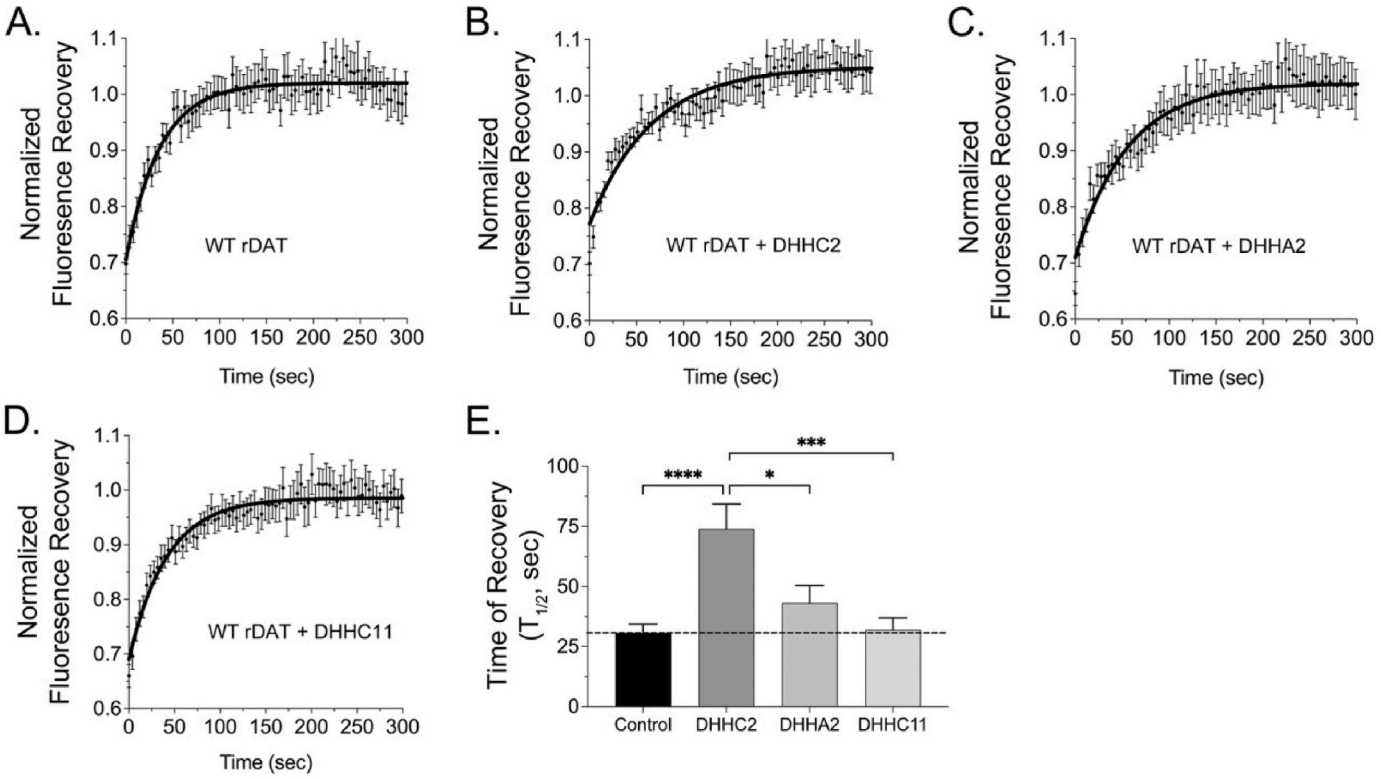

Fig. 6. Enhancement of palmitoylation decreases DAT lateral membrane mobility. N2a cells transiently transfected with EYFP-rDAT were co-transfected with empty vector (A), or coding plasmids for DHHC2 (B), DHHA2 (C) or DHHC11 (D) followed by FRAP analysis. Graphs show summary recovery curves (means ± S.E.) for independent experiments for each form. (E), Quantification of recovery times ($T_{1/2}$, sec) for each condition. (means ± S.E. of 3 or more independent experiments using 3 or more cells per experiment). *$p < 0.05$, ***$p < 0.001$, ****$p < 0.0001$, indicated conditions vs DHHC2 (one-way ANOVA with Tukey's post test).

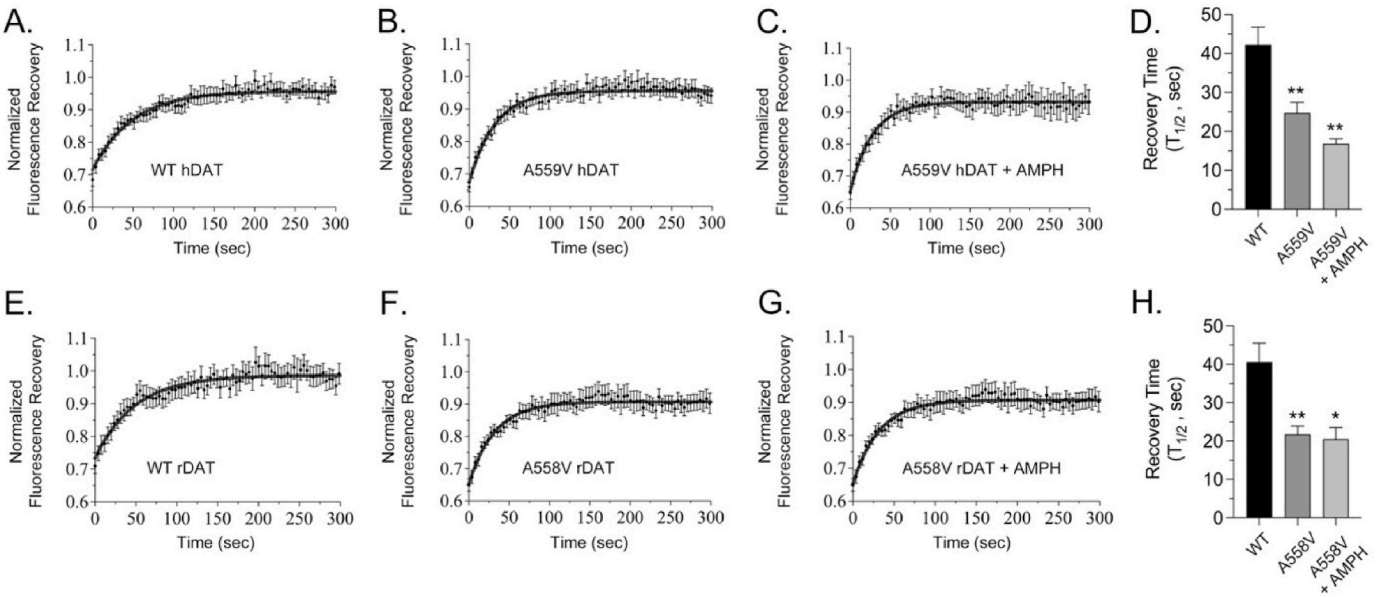

Fig. 7. A559V hDAT and A558V rDAT display increased, AMPH-insensitive lateral membrane mobility. N2a cells transiently expressing the indicated EYFP-hDAT forms (A–C) or EYFP-rDAT forms (E–G) were treated with vehicle (A, B, E, F) or AMPH (10 μM, 20 min) (C, G) and subjected to FRAP analysis. The graphs show summary recovery curves (means ± S.E.) for independent experiments for each condition. (D and H), Quantification of FRAP recovery times ($T_{1/2}$, sec). (means ± S.E. of 3 or more independent experiments using 3 or more cells/experiment). *$p < 0.05$, **$p < 0.01$ indicated conditions vs control (hDAT, one way ANOVA with Fisher's LSD post test; rDAT, one way ANOVA with Tukey's post test).

residues increases transporter lateral membrane mobility.

We then examined the role of DAT palmitoylation in membrane mobility (Fig. 4). To assess effects of palmitoylation in the WT transporter we treated cells with the DHHC inhibitor 2-bromopalmitate (2BP), which suppresses the tonic level of DAT palmitoylation (Foster and Vaughan, 2011). In hDAT control cells the FRAP $T_{½}$ was 41.6 ± 4.9 s

Table 1
Summary of EYFP-hDATmembrane characteristics for indicated experimental groups in N2a cells. N indicates total number of individual cells analyzed for each condition. Statistical tests refer to $T_{½}$ and D values. *p < 0.05, **p < 0.01, ***p < 0.001, ****p < 0.0001.

DAT Type	$T_{1/2}$ (sec)	D (x 10^{-3} μm^2/s)	N	Statistical Tests
hDAT	42.2 ± 4.6	3.3 ± 0.4	21	ANOVA
hDAT + PMA	21.4 ± 5.5**	7.7 ± 1.4***	9	Fisher's LSD
hDAT + AMPH	24.1 ± 4.5*	6.1 ± 1.1*	10	
hDAT	38.7 ± 4.6	3.8 ± 0.4	25	ANOVA
S7A hDAT	66.6 ± 11.1**	2.5 ± 0.3*	19	Fisher's LSD
S53A hDAT	53.9 ± 6.0*	2.3 ± 0.3*	22	
hDAT	41.6 ± 4.9	3.8 ± 0.6	20	Student's t
hDAT +2BP	20.1 ± 3.0**	7.1 ± 1.2**	13	
hDAT	45.4 ± 4.2	2.9 ± 0.3	30	Student's t
C581A hDAT	15.5 ± 1.9****	6.9 ± 0.9****	12	
hDAT	40.4 ± 3.4	3.3 ± 0.3	48	ANOVA
A559V hDAT	24.7 ± 2.7**	5.6 ± 0.5*	23	Fisher's LSD
A559V hDAT + AMPH	16.8 ± 1.2**	6.2 ± 0.6*	9	

Table 2
Summary of EYFP-rDAT membrane characteristics for indicated experimental groups in N2a cells. N indicates total number of individual cells analyzed for each condition. Statistical tests refer to $T_{½}$ and D values. *p < 0.05, **p < 0.01, ****p < 0.0001.

DAT Type	$T_{1/2}$ (sec)	D (x 10^{-3} μm^2/s)	N	Statistical Tests
rDAT	40.7 ± 4.9	3.6 ± 0.4	21	ANOVA
rDAT + PMA	17.6 ± 2.5**	7.1 ± 1.0***	13	Fisher LSD
rDAT + AMPH	18.9 ± 2.9**	6.9 ± 0.9**	10	
rDAT	38.2 ± 5.4	4.1 ± 0.5	19	Student's t
T53A rDAT	61.2 ± 10.5*	2.5 ± 0.4*	12	
rDAT	40.4 ± 6.7	4.1 ± 0.7	15	Student's t
rDAT + 2BP	14.7 ± 2.0*	7.1 ± 1.1*	10	
rDAT	40.4 ± 4.8	4.3 ± 0.5	36	Student's t
C580A rDAT	20.7 ± 2.5**	7.2 ± 1.0**	18	
rDAT	30.7 ± 3.6	4.7 ± 0.5	31	ANOVA
rDAT + DHHC2	74.0 ± 10.2****	2.0 ± 0.3**	22	Tukey
rDAT + DHHA2	42.5 ± 7.5	3.3 ± 0.5	20	
rDAT + DHHC11	32.0 ± 5.0	5.3 ± 0.7	25	
rDAT	41.3 ± 4.1	4.2 ± 0.4	48	ANOVA
A558V rDAT	21.8 ± 2.1**	6.1 ± 0.6**	22	Tukey
A558V rDAT + AMPH	20.5 ± 3.0*	7.1 ± 1.5**	10	

(Fig. 4A), and in cells treated with 2BP the $T_{½}$ was 20.1 ± 3.0 s (Fig. 4B) (p < 0.01 vs control) (Fig. 4C), indicating that transporters with reduced palmitoylation possess enhanced mobility. Similarly, the control $T_{½}$ value for rDAT was 40.4 ± 6.7 s (Fig. 4D) and for 2BP treatment was 14.7 ± 2.0 s (Fig. 4E) (p < 0.05 vs control) (Fig. 4F). 2BP also significantly increased the mobility of h/rDAT expressed in $LLCPK_1$ cells (Table 3).

Further testing of reduced DAT palmitoylation was performed using hDAT C581A and rDAT C580A forms, in which a major palmitoylation site has been removed (Fig. 5). Here the $T_{½}$ for WT hDAT was 45.4 ± 4.2 s (Fig. 5A) and for C581A DAT was 15.5 ± 1.9 s (Fig. 5B) (p < 0.0001) (Fig. C), indicating that transporters with elevated palmitoylatiion possess increased mobility. rDAT showed a similar pattern, with the $T_{½}$

Table 3
Summary of EYFP-h/rDAT membrane characteristics for indicated experimental groups in $LLCPK_1$ cells. N indicates total number of individual cells analyzed for each condition. Statistical tests refer to $T_{½}$ and D values. *p < 0.05, **p < 0.01, ***p < 0.001, ****p < 0.0001.

DAT Type	$T_{1/2}$ (sec)	D (x 10^{-3} μm^2/s)	N	Statistical Tests
rDAT	48.4 ± 4.8	2.4 ± 0.2	21	ANOVA
A558V rDAT	19.7 ± 2.0****	6.3 ± 0.7****	18	Tukey
rDAT + 2BP	32.3 ± 3.9*	4.4 ± 0.7*	14	
hDAT	50.1 ± 4.7	2.4 ± 0.2	21	ANOVA
A559V hDAT	25.9 ± 2.7***	6.3 ± 0.7****	19	Tukey
hDAT + 2BP	29.1 ± 4.7**	4.4 ± 0.7*	14	

for the WT form being 40.4 ± 4.8 s (Fig. 5D) and the C580A form being 20.7 ± 2.5 s (Fig. 5E) (p < 0.01 vs WT control) (Fig. 5F).

In Fig. 6 we examined responses to enhanced DAT palmitoylation. Here we utilized co-expression of rDAT with the palmitoyl acyltransferase DHHC2, which elevates transporter palmitoylation (Bolland et al., 2019). For WT rDAT cells co-transfected with empty vector (Fig. 6A) the FRAP $T_{½}$ was 30.7 ± 3.6 s and with DHHC2 co-transfection (Fig. 6B) the $T_{½}$ was 74.0 ± 10.2 s (p < 0.0001 vs control) (Fig. 6E), indicating reduced membrane mobility. In control experiments performed in parallel we co-transfected rDAT with the enzymatically inactive DHHA2 mutant or with DHHC11, which do not affect DAT palmitoylation (Bolland et al., 2019). The recovery $T_{½}$ was 42.5 ± 7.5 s for DHHA2 (Figs. 6C) and 32.0 ± 5.0 s for DHHC11 (Fig. 6D), values that are not different from control (p > 0.05) but are significantly different from DHHC2 (DHHA2, p < 0.05; DHHC11, p < 0.001) (Fig. 6E). Together these findings are consistent with palmitoylation functioning to reduce DAT membrane mobility.

In Fig. 7 we examined the properties of A559V hDAT and the rDAT homolog A558V in the absence and presence of AMPH. For hDAT (Fig. 7A) the recovery $T_{½}$ for the WT form was 40.4 ± 3.4 s and for A559V the $T_{½}$ was 24.7 ± 2.7 s (p < 0.01 vs control) (Fig. 7B), indicating enhanced mobility. When hDAT A559V cells were treated with AMPH (Fig. 7C) the $T_{½}$ was 16.8 ± 1.2 s, which is statistically different from WT (p < 0.01) but not from A559V (p > 0.05) (Fig. 7D), demonstrating that the endogenously enhanced mobility of this form is not further impacted by the drug. Similar results were obtained for rDAT, with $T_{½}$ values of 41.3 ± 4.1 s for WT DAT (Figs. 7E), 21.8 ± 2.1 s for A558V (Fig. 7F) (p < 0.01 vs WT), and 20.5 ± 3.0 s for A558V plus AMPH (Fig. 7G) (p < 0.05 vs WT; p > 0.05 vs A558V) (Fig. 7H). Endogenously enhanced mobility of A559/558V forms was also seen in $LLCPK_1$ cells (Table 3).

4. Discussion

These findings demonstrate that the membrane mobilities of rat and human DAT are regulated in a bidirectional manner, with diffusion increased by conditions that enhance phosphorylation or reduce palmitoylation (PKC, AMPH, A559V, 2BP, C580/581A) and reduced by conditions that enhance palmitoylation or reduce phosphorylation (DHHC2, S7A, S/T53A). This confirms and extends previous reports that showed PKC and AMPH enhancement of hDAT membrane mobility (Kovtun et al., 2019; Thal et al., 2019) and enhanced, PKC-insensitive mobility of A559V DAT that correlated with phosphorylation site mutations (Thal et al., 2019). Together these findings indicate that tonic membrane mobility derives from a balance between post-translational states that are under acute control by multiple presynaptic pathways.

These mobility properties can be incorporated into the model shown in Fig. 8, which summarizes the distribution of DAT between populations exhibiting high phosphorylation−low palmitoylation or low phosphorylation−high palmitoylation. We previously demonstrated this reciprocal pattern with respect to PKC domain/Ser7 phosphorylation and Cys580 palmitoylation and the regulatory outcomes associated with each condition (Moritz et al., 2015). Superimposition of FRAP findings

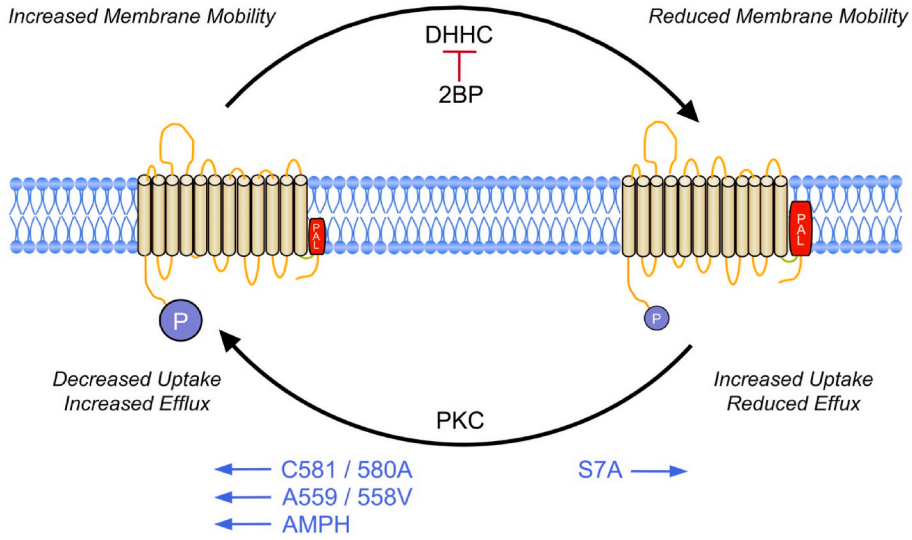

Fig. 8. Regulation of DAT membrane mobility by PKC domain phosphorylation and Cys580 palmitoylation. Model shows DAT populations enriched for high PKC domain phosphorylation−low Cys580 palmitoylation (left) or low PKC domain phosphorylation−high Cys580 palmitoylation (right), driven by the indicated PKC, DHHC, AMPH, and mutagenesis conditions. The diagram indicates the relationship between indicated conditions and mobility properties determined in this study, and uptake and efflux outcomes determined in previous studies.

with these populations indicates an inverse correlation between membrane mobility and transport activity, with increased mobility correlating with PKC domain phosphorylation and reduced transport, and decreased mobility correlating with Cys580 palmitoylation and increased transport (Fig. 8). These correlations do not include Thr53, as its mechanistic relationships, if any, to the other modifications are not known, and its regulation is associated with a distinct constellation of functions. The site undergoes enhanced phosphorylation by PKC and AMPH and phosphorylation-null forms show decreased mobility similar to the PKC domain responses, but when under the control of MAPK signaling the site functions to increase transport activity (Bolan et al., 2007; Foster et al., 2012; Gowrishankar et al., 2018; Mayer et al., 2023). The different responses of the modification sites thus support a specificity to mobility properties, possibly involving direction of DAT to distinct regulome or enzyme complexes.

The post-translational targets that mediate these mobility and functional outcomes could include both DAT and its regulatory partners, as enzyme and mutagenesis findings strongly support outcomes resulting directly from DAT modification, but the global pharmacological treatments likely induce impacts on binding partner modifications as well. Proteomic and lipidomic studies have identified a large number of cellular constiuents that interact with DAT (Maiya et al., 2007; Torres, 2006). Some of the more well-characterized regulatory partners include syntaxin 1A (Carvelli et al., 2008; Cervinski et al., 2010), flotillin 1 (Cremona et al., 2011; Sorkina et al., 2013), α-synuclein (Butler et al., 2015), endocytotic machinery (Fagan et al., 2020; Torres et al., 2001), and receptors and G-proteins (Garcia-Olivares et al., 2017; Lee et al., 2007; Thompson et al., 2000), all of which are subject to extensive post-translational control that could play roles in these mechanisms.

Considerable evidence now supports that direct phosphorylation of DAT at Ser7, Thr53, and other PKC domain residues drives kinetic control of reuptake via impacts on transporter conformational equilibrium, transport V_{max}, and tonic and AMPH-stimulated efflux (Bowton et al., 2010; Foster et al., 2012; Khoshbouei et al., 2004; Moritz et al., 2013, 2015). The contributions of binding partner modifications in these events has been less well-studied, but phosphorylation of flotillin 1 and syntaxin 1A impact or are implicated in PKC-stimulated efflux and DAT endocytosis (Cremona et al., 2011; Shekar et al., 2023). The interactome may also indirectly influence transporter phosphorylation mechanisms through enzyme recruitment or modification site accessibility, as syntaxin 1A, which binds to the transporter N-terminus (Lee et al., 2004), stabilizes tonic DAT phosphorylation in the absence of exogenous kinase or phosphatase treatments (Cervinski et al., 2010).

Less is known about the role of palmitoylation in these events, but many transporter partners including syntaxins, flotillins, receptors, and G-proteins are also palmitoylated (Kwiatkowska et al., 2020; Patwardhan et al., 2021), raising the possibility that enhanced hydrophobicity or structural impacts could drive binding interactions that reduce membrane mobility. Consistent with this idea, a recent modeling study shows that DAT dimerization, which is implicated in enhancement of transport (Cheng et al., 2017; Gur et al., 2017), is increased by Cys580 palmitoylation (Zeppelin et al., 2018), providing a possible mechanism for our findings of palmitoylation-induced transport upregulation (Bolland et al., 2019).

Links between membrane partitioning and DAT regulation have been found in other studies (Adkins et al., 2007; Eriksen et al., 2009; Kovtun et al., 2019; Thal et al., 2019), but the relationships between the various findings remain unclear. A significant fraction of DAT is partitioned into cholesterol-rich membrane rafts that represent sites for PKC-stimulated phosphorylation and by extension down-regulation and efflux. However, movement between raft and nonraft domains was not seen with PKC activation (Foster et al., 2008), and the relationship between cholesterol-based rafts and regulated FRAP mobility is not known. Transporters have also been shown by superresolution microscopy to undergo clustering into phosphatidyl inositol bisphosphate-enriched nanonanodomains, with movement between clustered and unclustered populations induced by various DAT regulatory signals including cholesterol, Ca^{2+}, and D2 DA receptors (Lycas et al., 2022; Rahbek-Clemmensen et al., 2017). Here cocaine analog binding indicated that clustered transporters reside in inwardly-facing conformations predicted to possess reduced transport kinetics and unclustered transporters reside in outwardly-facing conformations predicted to possess enhanced transport kinetics, but the relationship between these transporter populations and other microdomain or modification states is not known.

Membrane properties are thus closely intertwined with DAT function and regulation, and may be relevant to DA pathologies, as AMPH and the A559V variant induce enhanced lateral mobility that may contribute to dysregulated uptake. While the conditions examined in the present study were focused on acute regulatory conditions, these properties may also pertain to longer-term functionalities, as membrane mobility drives the transporter subcellular destination in neurons (Bagalkot et al., 2021), and PKC and palmitoylation mediate longer-term regulation of

total DAT levels that establish overall reuptake and signaling capacity via control of transporter entry into the degradation pathway (Bolland et al., 2019; Miranda et al., 2005).

Author contributions

RAV and JDF conceived and directed the project, analyzed the data, and wrote the paper. BDG and JM directed the FRAP studies; MS, DEB, and JM performed experiments, analyzed data, and assisted with writing.

Declaration of competing interest

The authors declare that they have no known competing financial interests or personal relationships that could have appeared to influence the work reported in this paper.

Data availability

Data will be made available on request.

Acknowledgments

This work was supported by the University of North Dakota and grants R15 DA031991 to JDF, P20 GM104360 to RAV, NSF ND EPSCoR Doctoral Dissertation Fellowship to DER; and P20 GM103442, P20GM113123, U54GM128729 to UND. We thank Dr. Masaki Fukata, National Institute for Physiological Sciences, Japan, for the generous gift of DHHC coding plasmids and Sarah Abrahamson for technical support and training for FRAP analysis.

References

Adkins, E.M., Samuvel, D.J., Fog, J.U., Eriksen, J., Jayanthi, L.D., Vaegter, C.B., Ramamoorthy, S., Gether, U., 2007. Membrane mobility and microdomain association of the dopamine transporter studied with fluorescence correlation spectroscopy and fluorescence recovery after photobleaching. Biochemistry 46, 10484–10497. https://doi.org/10.1021/bi700429z.

Bagalkot, T.R., Block, E.R., Bucchin, K., Balcita-Pedicino, J.J., Calderon, M., Sesack, S.R., Sorkin, A., 2021. Dopamine transporter localization in medial forebrain bundle axons indicates its long-range transport primarily by membrane diffusion with a limited contribution of vesicular traffic on retromer-positive compartments. J. Neurosci. 41, 234–250. https://doi.org/10.1523/JNEUROSCI.0744-20.2020.

Bermingham, D.P., Blakely, R.D., 2016. Kinase-dependent regulation of monoamine neurotransmitter transporters. Pharmacol. Rev. 68, 888–953. https://doi.org/10.1124/pr.115.012260.

Bolan, E.A., Kivell, B., Jaligam, V., Oz, M., Jayanthi, L.D., Han, Y., Sen, N., Urizar, E., Gomes, I., Devi, L.A., Ramamoorthy, S., Javitch, J.A., Zapata, A., Shippenberg, T.S., 2007. D2 receptors regulate dopamine transporter function via an extracellular signal-regulated kinases 1 and 2-dependent and phosphoinositide 3 kinase-independent mechanism. Mol. Pharmacol. 71, 1222–1232. https://doi.org/10.1124/mol.106.027763.

Bolland, D.E., Moritz, A.E., Stanislowski, D.J., Vaughan, R.A., Foster, J.D., 2019. Palmitoylation by multiple DHHC enzymes enhances dopamine transporter function and stability. ACS Chem. Neurosci. 10, 2707–2717. https://doi.org/10.1021/acschemneuro.8b00558.

Bowton, E., Saunders, C., Erreger, K., Sakrikar, D., Matthies, H.J., Sen, N., Jessen, T., Colbran, R.J., Caron, M.G., Javitch, J.A., Blakely, R.D., Galli, A., 2010. Dysregulation of dopamine transporters via dopamine D2 autoreceptors triggers anomalous dopamine efflux associated with attention-deficit hyperactivity disorder. J. Neurosci. 30, 6048–6057. https://doi.org/10.1523/JNEUROSCI.5094-09.2010.

Bowton, E., Saunders, C., Reddy, I.A., Campbell, N.G., Hamilton, P.J., Henry, L.K., Coon, H., Sakrikar, D., Veenstra-VanderWeele, J.M., Blakely, R.D., Sutcliffe, J., Matthies, H.J.G., Erreger, K., Galli, A., 2014. SLC6A3 coding variant Ala559Val found in two autism probands alters dopamine transporter function and trafficking. Transl. Psychiatry 4, e464. https://doi.org/10.1038/tp.2014.90.

Butler, B., Goodwin, S., Saha, K., Becker, J., Sambo, D., Davari, P., Khoshbouei, H., 2015. Dopamine transporter activity is modulated by α-synuclein. J. Biol. Chem. 290, 19009 https://doi.org/10.1074/jbc.A115.639880.

Carvelli, L., Blakely, R.D., DeFelice, L.J., 2008. Dopamine transporter/syntaxin 1A interactions regulate transporter channel activity and dopaminergic synaptic transmission. Proc. Natl. Acad. Sci. U. S. A. 105, 14192–14197. https://doi.org/10.1073/pnas.0802214105.

Cervinski, M.A., Foster, J.D., Vaughan, R.A., 2010. Syntaxin 1A regulates dopamine transporter activity, phosphorylation and surface expression. Neuroscience 170, 408–416. https://doi.org/10.1016/j.neuroscience.2010.07.025.

Cervinski, M.A., Foster, J.D., Vaughan, R.A., 2005. Psychoactive substrates stimulate dopamine transporter phosphorylation and down-regulation by cocaine-sensitive and protein kinase C-dependent mechanisms. J. Biol. Chem. 280, 40442 https://doi.org/10.1074/jbc.M501969200, 9.

Cervinski, M.A., Vaughan, R.A., 2005. Syntaxin 1A Mediates Phosphorylation and Regulation of the Dopamine Transporter. Abstract Viewer/Itinerary Planner. Society for Neuroscience Program, Washington, DC. No 39.8, Online.

Challasivakanaka, S., Zhen, J., Smith, M.E., Reith, M.E.A., Foster, J.D., Vaughan, R.A., 2017. Dopamine transporter phosphorylation site threonine 53 is stimulated by amphetamines and regulates dopamine transport, efflux, and cocaine analog binding. J. Biol. Chem. https://doi.org/10.1074/jbc.M117.787002.

Cheng, M.H., Garcia-Olivares, J., Wasserman, S., DiPietro, J., Bahar, I., 2017. Allosteric modulation of human dopamine transporter activity under conditions promoting its dimerization. J. Biol. Chem. 292, 12471–12482. https://doi.org/10.1074/jbc.M116.763565.

Cremona, M.L., Matthies, H.J., Pau, K., Bowton, E., Speed, N., Lute, B.J., Anderson, M., Sen, N., Robertson, S.D., Vaughan, R.A., Rothman, J.E., Galli, A., Javitch, J.A., Yamamoto, A., 2011. Flotillin-1 is essential for PKC-triggered endocytosis and membrane microdomain localization of DAT. Nat. Neurosci. 14, 469–477. https://doi.org/10.1038/nn.2781.

Eriksen, J., Rasmussen, S.G., Rasmussen, T.N., Vaegter, C.B., Cha, J.H., Zou, M.F., Newman, A.H., Gether, U., 2009. Visualization of dopamine transporter trafficking in live neurons by use of fluorescent cocaine analogs. J. Neurosci. 29, 6794–6808. https://doi.org/10.1523/jneurosci.4177-08.2009.

Fagan, R.R., Kearney, P.J., Sweeney, C.G., Luethi, D., Schoot Uiterkamp, F.E., Schicker, K., Alejandro, B.S., O'Connor, L.C., Sitte, H.H., Melikian, H.E., 2020. Dopamine transporter trafficking and Rit2 GTPase: mechanism of action and in vivo impact. J. Biol. Chem. 295, 5229–5244. https://doi.org/10.1074/jbc.RA120.012628.

Foster, J.D., Adkins, S.D., Lever, J.R., Vaughan, R.A., 2008. Phorbol ester induced trafficking-independent regulation and enhanced phosphorylation of the dopamine transporter associated with membrane rafts and cholesterol. J. Neurochem. 105, 1683–1699. https://doi.org/10.1111/j.1471-4159.2008.05262.x.

Foster, J.D., Pananusorn, B., Vaughan, R.A., 2002. Dopamine transporters are phosphorylated on N-terminal serines in rat striatum. J. Biol. Chem. 277, 25178–25186. https://doi.org/10.1074/jbc.M200294200.

Foster, J.D., Vaughan, R.A., 2017. Phosphorylation mechanisms in dopamine transporter regulation. J. Chem. Neuroanat. 83–84, 10–18. https://doi.org/10.1016/j.jchemneu.2016.10.004.

Foster, J.D., Vaughan, R.A., 2011. Palmitoylation controls dopamine transporter kinetics, degradation, and protein kinase C-dependent regulation. J. Biol. Chem. 286, 5175–5186. https://doi.org/10.1074/jbc.M110.187872.

Foster, J.D., Yang, J.-W., Moritz, A.E., Challasivakanaka, S., Smith, M.A., Holy, M., Wilebski, K., Sitte, H.H., Vaughan, R.A., 2012. Dopamine transporter phosphorylation site threonine 53 regulates substrate reuptake and amphetamine-stimulated efflux. J. Biol. Chem. 287, 29702–29712. https://doi.org/10.1074/jbc.M112.367706.

Fukata, M., Fukata, Y., Adesnik, H., Nicoll, R.A., Bredt, D.S., 2004. Identification of PSD-95 palmitoylating enzymes. Neuron 44, 987–996. https://doi.org/10.1016/j.neuron.2004.12.005.

Garcia-Olivares, J., Baust, T., Harris, S., Hamilton, P., Galli, A., Amara, S.G., Torres, G.E., 2017. Gβγ subunit activation promotes dopamine efflux through the dopamine transporter. Mol. Psychiatr. 22, 1673–1679. https://doi.org/10.1038/mp.2017.176.

Giros, B., Jaber, M., Jones, S.R., Wightman, R.M., Caron, M.G., 1996. Hyperlocomotion and indifference to cocaine and amphetamine in mice lacking the dopamine transporter. Nature 379, 606–612. https://doi.org/10.1038/379606a0.

Gowrishankar, R., Gresch, P.J., Davis, G.L., Katamish, R.M., Riele, J.R., Stewart, A.M., Vaughan, R.A., Hahn, M.K., Blakely, R.D., 2018. Region-specific regulation of presynaptic dopamine homeostasis by D2 autoreceptors shapes the in vivo impact of the neuropsychiatric disease-associated DAT variant Val 559. J. Neurosci. 38, 5302–5312. https://doi.org/10.1523/JNEUROSCI.0055-18.2018.

Gur, M., Cheng, M.H., Zomot, E., Bahar, I., 2017. Effect of dimerization on the dynamics of neurotransmitter:sodium symporters. J. Phys. Chem. B 121, 3657–3666. https://doi.org/10.1021/acs.jpcb.6b09876.

Huff, R.A., Vaughan, R.A., Kuhar, M.J., Uhl, G.R., 1997. Phorbol esters increase dopamine transporter phosphorylation and decrease transport Vmax. J. Neurochem. 68, 225–232. https://doi.org/10.1046/j.1471-4159.1997.68010225.x.

Kang, M., Day, C.A., Kenworthy, A.K., DiBenedetto, E., 2012. Simplified equation to extract diffusion coefficients from confocal FRAP data. Traffic 13, 1589–1600. https://doi.org/10.1111/tra.12008.

Khelashvili, G., Weinstein, H., 2015. Functional mechanisms of neurotransmitter transporters regulated by lipid-protein interactions of their terminal loops. Biochim. Biophys. Acta 1848, 1765–1774. https://doi.org/10.1016/j.bbamem.2015.03.025.

Khoshbouei, H., Sen, N., Guptaroy, B., Johnson, L., Lund, D., Gnegy, M.E., Galli, A., Javitch, J.A., 2004. N-terminal phosphorylation of the dopamine transporter is required for amphetamine-induced efflux. PLoS Biol. 2, E78.

Kovtun, O., Tomlinson, I.D., Ferguson, R.S., Rosenthal, S.J., 2019. Quantum dots reveal heterogeneous membrane diffusivity and dynamic surface density polarization of dopamine transporter. PLoS One 14, e0225339. https://doi.org/10.1371/journal.pone.0225339.

Kwiatkowska, K., Matveichuk, O.V., Fronk, J., Ciesielska, A., 2020. Flotillins: at the intersection of protein S-palmitoylation and lipid-mediated signaling. Int. J. Mol. Sci. 21, 2283. https://doi.org/10.3390/ijms21072283.

Lee, K.H., Kim, M.Y., Kim, D.H., Lee, Y.S., 2004. Syntaxin 1A and receptor for activated C kinase interact with the N-terminal region of human dopamine transporter.

Neurochem Res 29, 1405–1409. https://doi.org/10.1023/B:NERE.0000026404.08779.43.
Lee, F.J., Pei, L., Moszczynska, A., Vukusic, B., Fletcher, P.J., Liu, F., 2007. Dopamine transporter cell surface localization facilitated by a direct interaction with the dopamine D2 receptor. EMBO J. 26, 2127–2136. https://doi.org/10.1038/sj.emboj.7601656.
Lycas, M.D., Ejdrup, A.L., Sørensen, A.T., Haahr, N.O., Jørgensen, S.H., Guthrie, D.A., Støier, J.F., Werner, C., Newman, A.H., Sauer, M., Herborg, F., Gether, U., 2022. Nanoscopic dopamine transporter distribution and conformation are inversely regulated by excitatory drive and D2 autoreceptor activity. Cell Rep. 40, 111431 https://doi.org/10.1016/j.celrep.2022.111431.
Maiya, R., Ponomarev, I., Linse, K.D., Harris, R.A., Mayfield, R.D., 2007. Defining the dopamine transporter proteome by convergent biochemical and in silico analyses. Gene Brain Behav. 6, 97–106. https://doi.org/10.1111/j.1601-183X.2006.00236.x.
Mayer, F.P., Stewart, A., Varman, D.R., Moritz, A.E., Foster, J.D., Owens, A.W., Areal, L. B., Gowrishankar, R., Velez, M., Wickham, K., Phelps, H., Katamish, R., Rabil, M.J., Jayanthi, L.D., Vaughan, R.A., Daws, L.C., Blakely, R., Ramamoorthy, S., 2023. Kappa opioid receptor antagonism rescues genetic perturbation of dopamine homeostasis. Molecular, Physiological and Behavioral Consequences. https://doi.org/10.1101/2023.05.03.539310.
Miranda, M., Wu, C.C., Sorkina, T., Korstjens, D.R., Sorkin, A., 2005. Enhanced ubiquitylation and accelerated degradation of the dopamine transporter mediated by protein kinase C. J. Biol. Chem. 280, 35617–35624. https://doi.org/10.1074/jbc.M506618200.
Moritz, A.E., Foster, J.D., Gorentla, B.K., Mazei-Robison, M.S., Yang, J.W., Sitte, H.H., Blakely, R.D., Vaughan, R.A., 2013. Phosphorylation of dopamine transporter serine 7 modulates cocaine analog binding. J. Biol. Chem. 288, 20–32. https://doi.org/10.1074/jbc.M112.407874.
Moritz, A.E., Rastedt, D.E., Stanislowski, D.J., Shetty, M., Smith, M.A., Vaughan, R.A., Foster, J.D., 2015. Reciprocal phosphorylation and palmitoylation control dopamine transporter kinetics. J. Biol. Chem. 290, 29095–29105. https://doi.org/10.1074/jbc.M115.667055.
Nirenberg, M.J., Vaughan, R.A., Uhl, G.R., Kuhar, M.J., Pickel, V.M., 1996. The dopamine transporter is localized to dendritic and axonal plasma membranes of nigrostriatal dopaminergic neurons. J. Neurosci. 16, 436–447. https://doi.org/10.1523/JNEUROSCI.16-02-00436.1996.
Patwardhan, A., Cheng, N., Trejo, J., 2021. Post-translational modifications of G protein-coupled receptors control cellular signaling dynamics in space and time. Pharmacol. Rev. 73, 120–151. https://doi.org/10.1124/pharmrev.120.000082.
Piniella, D., Martínez-Blanco, E., Bartolomé-Martín, D., Sanz-Martos, A.B., Zafra, F., 2021. Identification by proximity labeling of novel lipidic and proteinaceous potential partners of the dopamine transporter. Cell. Mol. Life Sci. 78, 7733–7756. https://doi.org/10.1007/s00018-021-03998-1.
Rahbek-Clemmensen, T., Lycas, M.D., Erlendsson, S., Eriksen, J., Apuschkin, M., Vilhardt, F., Jørgensen, T.N., Hansen, F.H., Gether, U., 2017. Super-resolution microscopy reveals functional organization of dopamine transporters into cholesterol and neuronal activity-dependent nanodomains. Nat. Commun. 8, 740. https://doi.org/10.1038/s41467-017-00790-3.
Rastedt, D.E., Vaughan, R.A., Foster, J.D., 2017. Palmitoylation mechanisms in dopamine transporter regulation. J. Chem. Neuroanat. 83–84, 3–9. https://doi.org/10.1016/j.jchemneu.2017.01.002.
Schmitt, K.C., Reith, M.E., 2010. Regulation of the dopamine transporter: aspects relevant to psychostimulant drugs of abuse. Ann. N. Y. Acad. Sci. 1187, 316–340. https://doi.org/10.1111/j.1749-6632.2009.05148.x.
Shekar, A., Mabry, S.J., Cheng, M.H., Aguilar, J.I., Patel, S., Zanella, D., Saleeby, D.P., Zhu, Y., Romanazzi, T., Ulery-Reynolds, P., Bahar, I., Carter, A.M., Matthies, H.J.G., Galli, A., 2023. Syntaxin 1 Ser 14 phosphorylation is required for nonvesicular dopamine release. Sci. Adv. 9, eadd8417 https://doi.org/10.1126/sciadv.add8417.
Sorkina, T., Caltagarone, J., Sorkin, A., 2013. Flotillins regulate membrane mobility of the dopamine transporter but are not required for its protein kinase C dependent endocytosis. Traffic 14, 709–724. https://doi.org/10.1111/tra.12059.
Thal, L.B., Tomlinson, I.D., Quinlan, M.A., Kovtun, O., Blakely, R.D., Rosenthal, S.J., 2019. Single quantum dot imaging reveals PKCβ-dependent alterations in membrane diffusion and clustering of an attention-deficit hyperactivity disorder/autism/bipolar disorder-associated dopamine transporter variant. ACS Chem. Neurosci. 10, 460–471. https://doi.org/10.1021/acschemneuro.8b00350.
Thompson, A.C., Zapata, A., Justice, J.B., Vaughan, R.A., Sharpe, L.G., Shippenberg, T.S., 2000. Kappa-opioid receptor activation modifies dopamine uptake in the nucleus accumbens and opposes the effects of cocaine. J. Neurosci. 20, 9333–9340. https://doi.org/10.1523/JNEUROSCI.20-24-09333.2000.
Torres, G.E., 2006. The dopamine transporter proteome. J. Neurochem. 97 (Suppl. 1), 3–10.
Torres, G.E., Yao, W.D., Mohn, A.R., Quan, H., Kim, K.M., Levey, A.I., Staudinger, J., Caron, M.G., 2001. Functional interaction between monoamine plasma membrane transporters and the synaptic PDZ domain-containing protein PICK1. Neuron 30, 121–134. https://doi.org/10.1016/S0896-6273(01)00267-7.
Vaughan, R.A., Foster, J.D., 2013. Mechanisms of dopamine transporter regulation in normal and disease states. Trends Pharmacol. Sci. 34, 489–496. https://doi.org/10.1016/j.tips.2013.07.005.
Wang, Q., Bubula, N., Brown, J., Wang, Y., Kondev, V., Vezina, P., 2016. PKC phosphorylates residues in the N-terminal of the DA transporter to regulate amphetamine-induced DA efflux. Neurosci. Lett. 622, 78–82. https://doi.org/10.1016/j.neulet.2016.04.051.
Wetzker, R., Böhmer, F.-D., 2003. Transactivation joins multiple tracks to the ERK/MAPK cascade. Nat. Rev. Mol. Cell Biol. 4, 651–657. https://doi.org/10.1038/nrm1173.
Yang, J.-W., Larson, G., Konrad, L., Shetty, M., Holy, M., Jäntsch, K., Kastein, M., Heo, S., Erdem, F.A., Lubec, G., Vaughan, R.A., Sitte, H.H., Foster, J.D., 2019. Dephosphorylation of human dopamine transporter at threonine 48 by protein phosphatase PP1/2A up-regulates transport velocity. J. Biol. Chem. 294, 3419–3431. https://doi.org/10.1074/jbc.RA118.005251.
Zeppelin, T., Ladefoged, L.K., Sinning, S., Periole, X., Schiøtt, B., 2018. A direct interaction of cholesterol with the dopamine transporter prevents its out-to-inward transition. PLoS Comput. Biol. 14, e1005907 https://doi.org/10.1371/journal.pcbi.1005907.